Navarro et al. BMC Biology (2016) 14:26
DOI 10.1186/s12915-016-0247-4

BMC Biology

RESEARCH ARTICLE Open Access

Quaternary structure of a G-protein-coupled receptor heterotetramer in complex with G_i and G_s

Gemma Navarro[1,2,3†], Arnau Cordomí[4†], Monika Zelman-Femiak[5,6†], Marc Brugarolas[1,2,3], Estefania Moreno[1,2,3], David Aguinaga[1,2,3], Laura Perez-Benito[4], Antoni Cortés[1,2,3], Vicent Casadó[1,2,3], Josefa Mallol[1,2,3], Enric I. Canela[1,2,3], Carme Lluís[1,2,3], Leonardo Pardo[4†], Ana J. García-Sáez[5,6,7†], Peter J. McCormick[1,2,3,8*†] and Rafael Franco[1,2,3*†]

Abstract

Background: G-protein-coupled receptors (GPCRs), in the form of monomers or homodimers that bind heterotrimeric G proteins, are fundamental in the transfer of extracellular stimuli to intracellular signaling pathways. Different GPCRs may also interact to form heteromers that are novel signaling units. Despite the exponential growth in the number of solved GPCR crystal structures, the structural properties of heteromers remain unknown.

Results: We used single-particle tracking experiments in cells expressing functional adenosine A_1-A_{2A} receptors fused to fluorescent proteins to show the loss of Brownian movement of the A_1 receptor in the presence of the A_{2A} receptor, and a preponderance of cell surface 2:2 receptor heteromers (dimer of dimers). Using computer modeling, aided by bioluminescence resonance energy transfer assays to monitor receptor homomerization and heteromerization and G-protein coupling, we predict the interacting interfaces and propose a quaternary structure of the GPCR tetramer in complex with two G proteins.

Conclusions: The combination of results points to a molecular architecture formed by a rhombus-shaped heterotetramer, which is bound to two different interacting heterotrimeric G proteins (G_i and G_s). These novel results constitute an important advance in understanding the molecular intricacies involved in GPCR function.

Keywords: GPCR, Heterotetramer, Heterotrimeric G protein, Single-particle tracking, BRET, Molecular modeling

Background

G-protein-coupled receptor (GPCR) oligomerization is heavily supported by recent biochemical and structural data [1–6]. Optical-based techniques are instrumental in studying the dynamics and organization of receptor complexes in living cells [7]. For instance, total internal reflection fluorescence microscopy shows that 30 % of muscarinic M1 receptors exist as dimers (with no evidence of higher oligomers) that undergo interconversion with monomers on a timescale of seconds [8]. Similarly, the β_1-adrenergic receptors (β_1-AR) are expressed as a mixture of monomers and dimers whereas β_2-adrenergic receptors (β_2-AR) have a tendency to form dimers and higher-order oligomers [9]. Moreover, the monomer-dimer equilibrium of the chemoattractant *N-formyl* peptide receptor at a physiological level of expression lies within a timescale of milliseconds [10]. Together, these studies in heterologous systems show that a given GPCR is present in a dynamic equilibrium between monomers, dimers, and higher-order oligomers.

Studies in a broad spectrum of GPCRs [11–14] show that these receptors may form heteromers. GPCR heteromers are defined as novel signaling units with functional properties different from homomers and they represent a completely new field of study [15]. Innovative crystallographic techniques have permitted researchers to obtain crystal structures of GPCR families A, B, C, and F, bound to either agonists, antagonists, inverse agonists or allosteric modulators; in the form of monomers or homo-oligomers; and in complex with a G protein or

* Correspondence: p.mccormick@uea.ac.uk; rfranco123@gmail.com
†Equal contributors
[1]Centro de Investigación Biomédica en Red sobre Enfermedades Neurodegenerativas (CIBERNED), Madrid, Spain
Full list of author information is available at the end of the article

with a ß-arrestin [16]. However, crystal structures of GPCR heteromers have not yet been obtained. Here, we propose a quaternary structure of a heteromer, taking into account the molecular stoichiometry and the interacting G proteins. Adenosine A_1-A_{2A} receptor (A_1R-$A_{2A}R$) complexes constitute a paradigm in the GPCR heteromer field because A_1R is coupled to G_i and $A_{2A}R$ to G_s; that is, they transduce opposite signals in cyclic adenosine monophosphate (cAMP)-dependent intracellular cascades. First described as a concentration-sensing device in striatal glutamatergic neurons [17], the A_1R-$A_{2A}R$ heteromer is thought to function as a G_s/G_i-mediated switching mechanism by which low and high concentrations of adenosine inhibit and stimulate, respectively, glutamate release [17, 18]. The structural basis of this switch is key to understanding heteromer function and the biological advantage behind the GPCR heteromerization phenomenon. Here, we have devised the molecular architecture of the adenosine A_1R-$A_{2A}R$ heteromer in complex with G proteins using a combination of microscope-based single-particle tracking, molecular modeling, and energy transfer assays in combination with molecular complementation. The results point to A_1 and A_{2A} receptors organizing into a rhombus-shaped heterotetramer that couples to G_i and G_s. The overall structure is very compact and provides interacting interfaces for GPCRs and for G proteins.

Results and discussion

Reciprocal restriction of adenosine receptor motion in the plasma membrane

To examine the dynamics of A_1R-$A_{2A}R$ heteromers in the plasma membrane of a living cell, the motion of the receptors tagged with fluorescent proteins (A_1R-green fluorescent protein [GFP] or $A_{2A}R$-mCherry) was measured by real-time single-particle tracking (SPT) (Fig. 1). Examples of fluorescent images and individual particle trajectories are shown in Additional file 1: Figure S1. Analysis of data corresponding to 500 A_1R-GFP particles showed a linear relationship between the mean square displacement (MSD) versus time lag in the trajectories of up to 1600 single fluorescent particles (Fig. 1a, c). This is typical for Brownian diffusion, indicating a lack of restrictions in A_1R-GFP motion. Co-expression of $A_{2A}R$-mCherry (Fig. 1b) led to a reduction in the lateral mobility of A_1R-GFP, which became confined to plasma membrane regions of 0.461 ± 0.004 μm in diameter. Its diffusion coefficient decreased from 0.381 ± 0.002 $\mu m^2/s$ to 0.291 ± 0.003 $\mu m^2/s$ ($p = 0.002$, one-tailed t-test). Similarly, A_1R-GFP also decreased the $A_{2A}R$-mCherry diffusion coefficient from 0.317 ± 0.002 $\mu m^2/s$ to 0.143 ± 0.005 $\mu m^2/s$ ($p < 0.0001$) (Fig. 1d–f). $A_{2A}R$ moved within a confinement zone of 0.941 ± 0.007 μm in diameter that was reduced to 0.360 ± 0.001 μm ($p < 0.0001$) when both receptors were co-expressed. We conclude from these mobility comparisons that reciprocally restricted motion of the individual receptor particles must be due to A_1R-$A_{2A}R$ receptor-receptor interactions.

Stoichiometry of A_1 and A_{2A} receptor heterocomplexes

The stoichiometry of the fluorescent receptors on the cell surface can be calculated from the brightness distribution of the individual particles [19] (see "Methods"). In cells expressing A_1R-GFP, we found the majority of clusters to consist of either two (~47 %) or four (~34 %) receptors, and clusters with one or three receptors were scarce (~10 % and ~9 %, respectively) (Additional file 2: Figure S2A and black bars in Additional file 2: Figure S2C). In the case of $A_{2A}R$-mCherry, the stoichiometry analysis showed that the clusters mostly expressed trimers (45 %), with dimers (29 %) and tetramers (12 %) the second and third most common populations (Additional file 2: Figure S2D and black bars in Additional file 2: Figure S2F). Remarkably, this stoichiometry for either A_1 or A_{2A} receptors was altered when the partner receptor was also expressed. In cells co-expressing A_1R-GFP and $A_{2A}R$-mCherry, the dimer population increased (57 % for A_1R-GFP and 49 % for $A_{2A}R$-mCherry, blue bars in Additional file 2: Figures S2C, F) and became the predominant species (Additional file 2: Figures S2B, C, E, F).

In order to focus the analysis on heteromer complexes, we identified clusters containing both receptors (individual yellow dots in Fig. 1g, displaying both GFP and mCherry fluorescence). In ~1000 analyzed co-localized clusters that consisted of a mixture of A_1-GFP and A_{2A}-Cherry (yellow dots in Fig. 1g), we found a similar high amount of dimers of A_1R (75 %, left panel in Fig. 1h and green bar in Fig. 1i) and $A_{2A}R$ (74 %, right panel in Fig. 1h and red bar in Fig. 1i). Trimers and tetramers of A_1R, and monomers and tetramers of $A_{2A}R$, were in the minority or negligible (see Fig. 1h, i). In summary, given that the percentage of dimers of either A_1R-GFP or $A_{2A}R$-mCherry in the yellow dots (which show co-localization of the two receptors) was similar and high (~75 %), the heterotetramer containing two A_1Rs and two $A_{2A}R$s must have been the most predominant species. To our knowledge, this is the first stoichiometry data for a GPCR heteromer in living cells.

Arrangement of G proteins interacting with A_1 and A_{2A} receptors

Monomeric GPCRs are capable of activating G proteins [20]. However, recent findings suggest that one GPCR homodimer bound to a single G protein may be a common functional unit [21]. Thus, an emerging question is how G proteins couple to GPCR heteromers. Because A_1R selectively couples to G_i and $A_{2A}R$ to G_s [22], the

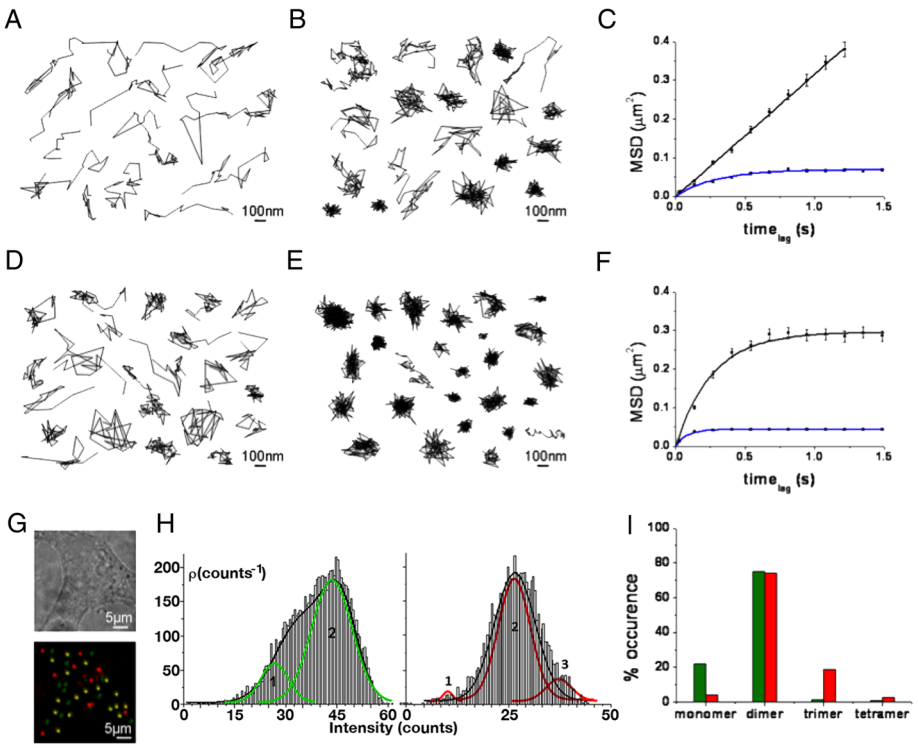

Fig. 1 Cell surface mobility of A_1R-GFP and A_{2A}R-mCherry. Individual trajectories of particles containing GFP fused to the C-terminus of A_1R (A_1-GFP) (**a** and **b**) or mCherry fused to the C-terminus of A_{2A}R (A_{2A}-mCherry) (**d** and **e**) on HEK-293T cells expressing A_1-GFP (a), A_{2A}-mCherry (d) or both (b and e). The trajectory and the fluorescence intensity of the individual particles were recorded over time using total internal reflection microscopy (TIRFM) and an electron multiplying charged-coupled device (EMCCD) camera recording. Receptor motion was determined by plotting (versus time lag) the mean square displacement (*MSD*) of A_1-GFP (**c**) in the absence (*black line*) or presence of A_{2A}-mCherry (*blue line*), or A_{2A}-mCherry (**f**) in the presence (*black line*) or presence of A_1-GFP (*blue line*). Data sets were fitted to mathematical models of free and confined diffusion for A_1R and A_{2A}R respectively. **g** Co-localization of A_1-GFP and A_{2A}-mCherry is observed (*yellow dots*). Scale bar: 100 nm. **h** Distribution of the fluorescence signal of A_1-GFP (*left*) and A_{2A}-mCherry (*right*) within co-localized receptors (*yellow dots* in g). Curves approximately delineate the number of monomers, dimers, or trimers within the co-localized complex. **i** Stoichiometry analysis performed for co-localized A_1-GFP and A_{2A}-mCherry receptor particles co-expressed in HEK-293T cells (*yellow dots* in g). *Green* corresponds to A_1-GFP and *red* to A_{2A}-mCherry

working hypothesis was that both G_i and G_s proteins may couple to the A_1R-A_{2A}R heterotetramer. To test this hypothesis, we used bioluminescence resonance energy transfer (BRET) assays [23]. In agreement with the SPT experiments (see above), homodimers and heterodimers were detected by BRET assays in cells expressing A_1R fused with *Renilla* luciferase (A_1R-Rluc) or yellow fluorescent protein (A_1R-YFP) (Fig. 2a), A_{2A}R-Rluc and A_{2A}R-YFP (Fig. 2b), or A_1R-Rluc and A_{2A}R-YFP (Fig. 2e). Neither A_1R-Rluc nor A_{2A}R-YFP interacted with the ghrelin receptor 1a fused to YFP (GHS1a-YFP), used as a control as a protein unable to directly interact with these adenosine receptors (Fig. 2a, b). In order to test the presence of the two G proteins in the heterotetramer, we transfected cells with minigenes that code for peptides blocking either G_i or G_s binding to GPCRs [24]. In addition, cells were treated with pertussis or cholera toxins that catalyze ADP-ribosylation of G_i or G_s. Clearly, treating cells with pertussis toxin, or expressing the minigene-coded peptide that blocks α_i coupling, reduced the value of $BRET_{max}$ for A_1R-A_1R homodimers (Fig. 2a) and for A_1R-A_{2A}R heterodimers (Fig. 2e) but not for A_{2A}R-A_{2A}R homodimers (Fig. 2b). This indicates that G_i is coupled to A_1R in both the homodimer and the heterodimer. Similarly, blocking G_s-receptor interaction using cholera toxin or a minigene-coded peptide that blocks α_S coupling reduced $BRET_{max}$ for A_{2A}R-A_{2A}R homodimers (Fig. 2b) and for A_1R-A_{2A}R heterodimers (Fig. 2e) but not for A_1R-A_1R homodimers (Fig. 2a). Interestingly, BRET curves showed sensitivity to both cholera and pertussis toxins in cells expressing either A_1R-Rluc-A_1R-YFP and A_{2A}R (Fig. 2c) or A_{2A}R-Rluc-A_{2A}R-YFP and A_1R (Fig. 2d). Functionality of constructs and controls in cells expressing minigenes, and in cells expressing the ghrelin GHS1a receptor instead of one of the adenosine receptors, are shown in Additional file 3: Figure S3. To further confirm that G_i binds A_{2A}R in the receptor heteromer, the energy transfer between Rluc fused to the N-terminal domain of the α-subunit of G_i (G_i-Rluc) and A_{2A}R-YFP was analyzed in

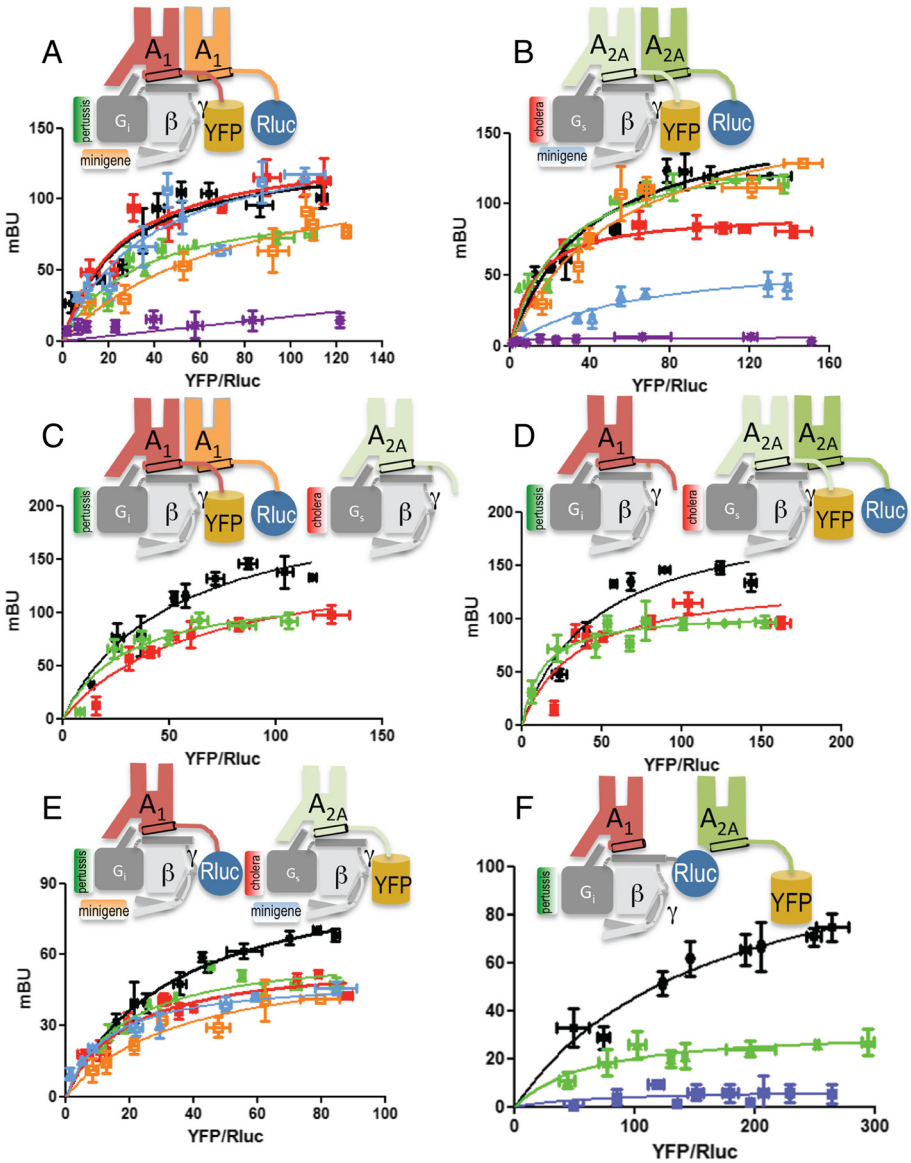

Fig. 2 Influence of G proteins on A_1R and $A_{2A}R$ homodimerization and heterodimerization. B Bioluminescence resonance energy transfer (BRET) saturation curves were performed in HEK-293T cells 48 h post-transfection with (**a**, **c**) 0.3 μg of cDNA corresponding to A_1R-Rluc and increasing amounts of A_1R-YFP (0.1–1.5 μg cDNA) or GHS1a-YFP (0.25–2 μg cDNA) as negative control (a, *purple line*), without (a) or with (c) 0.15 μg of cDNA corresponding to $A_{2A}R$; (**b**, **d**) 0.2 μg of cDNA corresponding to $A_{2A}R$-Rluc and increasing amounts of $A_{2A}R$-YFP (0.1–1.0 μg cDNA) or GHS1a-YFP (0.25–2 μg cDNA) as negative control (b, *purple line*), without (b) or with (d) 0.5 μg of cDNA corresponding to A_1R; (**e**) 0.3 μg of cDNA corresponding to A_1R-Rluc and increasing amounts of A_{2AR}-YFP (0.1–1.0 μg cDNA); and (**f**) 0.5 μg of cDNA corresponding to A_1R (except control *blue curves* that were obtained in cells not expressing A_1R), 2 μg of cDNA corresponding to G_i-Rluc, and increasing amounts of $A_{2A}R$-YFP (0.1–0.5 μg cDNA). In panels a, b, and e, cells were also transfected with 0.5 μg of cDNA corresponding to the G_i-related (*orange curves*) or G_s-related (*blue curves*) minigenes. Cells were treated for 16 h with medium (*black curves*), with 10 ng/ml of pertussis toxin (*green curves*), or with 100 ng/ml of cholera toxin (*red curves*) prior to BRET determination. To confirm similar donor expressions (approximately 100,000 bioluminescence units) while monitoring the increase in acceptor expression (1000–40,000 fluorescence units), the fluorescence and luminescence of each sample were measured before energy transfer data acquisition. MiliBRET unit (*mBU*) values are the mean ± standard error of the mean of four to six different experiments grouped as a function of the amount of BRET acceptor. In each panel (*top*) a cartoon depicts the proteins to which Rluc and YFP were fused and the presence or not of partner receptors and/or G_s or G_i proteins [schemes in c to f are not intended to illustrate on stoichiometry because the predominant form in cells expressing the two receptors was the heterotetramer containing two A_1 and two A_{2A} receptors (see "Results")]

cells co-expressing or not co-expressing A_1R (Fig. 2f). A hyperbolic BRET curve was observed in the presence of A_1R, but not in its absence, indicating that G_i and G_s are bound to their respective receptor homodimers within the A_1R-$A_{2A}R$ heteromer.

Further, two complementary BRET experiments were performed to determine the orientation of G_i and G_s within the A_1R-$A_{2A}R$ heterocomplex. First, Rluc and YFP were respectively fused to the N-terminal domains of the α-subunit of G_i (α_i-Rluc) and G_s (α_s-YFP) (Fig. 3, bar a); second, they were fused to the N-terminal domain of the γ-subunit (γ-Rluc and γ-YFP) (Fig. 3, bar b). We observed significant energy transfer between γ-Rluc and γ-YFP in cells co-expressing A_1R and $A_{2A}R$ (Fig. 3, bar b) but minimal amounts in negative-control cells (Fig. 3, bars c and d). In cells expressing either A_1R or $A_{2A}R$, the energy transfer between γ-Rluc and γ-YFP was also low (Fig. 3, bars e and f), suggesting that dimers but not tetramers were the most prevalent form of surface receptors in single-transfected cells. These results in co-transfected cells corroborate the 2:2 stoichiometry obtained from analysis of the fluorescence in single particles and are consistent with G_i and G_s binding to these A_1R-$A_{2A}R$ heterotetramers.

Molecular model of G_i and G_s bound to the A_1R-$A_{2A}R$ heterotetramer

To identify the orientation of the G protein in the receptor homodimer, we combined energy transfer assays between α_s-Rluc (Rluc at the N-terminus of the G protein α-subunit) and $A_{2A}R$-YFP (Fig. 4a) with information on transmembrane (TM) interfaces based on crystal structures of GPCRs [3, 4], which have been recently summarized [25]. The observed high-energy transfer using α_s-Rluc and $A_{2A}R$-YFP indicated close proximity between the N-tail of the α-subunit of G_s and the C-tail of $A_{2A}R$. Interestingly, Rluc and YFP in the "monomeric" $A_{2A}R$-G_s complex (see "Methods") point toward distant positions in space (Fig. 4b). Therefore, the observed BRET should occur between Rluc in the G protein α-subunit and a second $A_{2A}R$-YFP protomer. Among all described TM interfaces for receptor homodimerization (see Additional file 4: Figure S4), we propose the TM4/5 interface, which is observed in the oligomeric structure of β_1-AR [4] and in structures derived from coarse-grained molecular dynamics (MD) simulations [26]. In fact, this is the only interface that favors BRET between α_s-Rluc and a second $A_{2A}R$-YFP protomer in a homodimer (Fig. 4c). The homologous A_1R homodimer was built using the same TM4/5 interface as for $A_{2A}R$ (see Additional file 4: Figure S4 and its legend).

The remaining possible TMs able to form heteromeric interfaces are TM1 and TM5/6 (Fig. 5). Both are possible inter-GPCR interfaces as observed in the structure of the μ-opioid receptor (μ-OR) [3]. To discern between these two possibilities, a bimolecular fluorescence complementation strategy was undertaken. For this purpose,

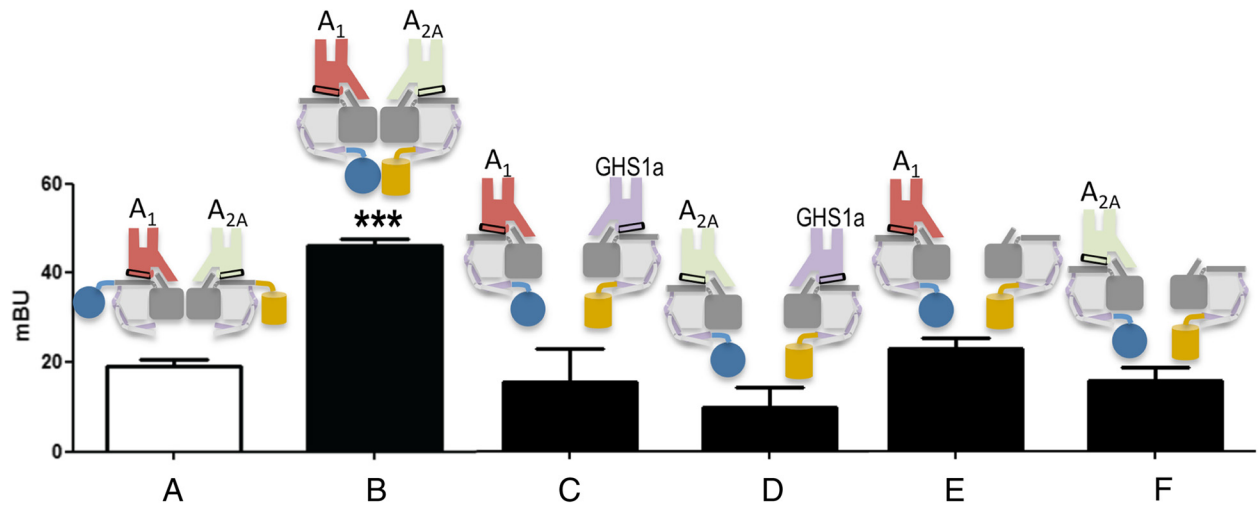

Fig. 3 G_s and G_i coupling to adenosine A_1R-$A_{2A}R$ heterocomplexes. Bioluminescence resonance energy transfer (BRET) experiments were performed in HEK-293T cells 48 h post-transfection with (**a**, **b**) 0.2 μg of cDNA corresponding to A_1R and 0.15 μg of cDNA corresponding to $A_{2A}R$; (**c**, **d**) 0.2 μg of cDNA corresponding to A_1R or 0.15 μg of cDNA corresponding to $A_{2A}R$ and 0.4 μg of cDNA corresponding to growth hormone secretagogue receptor GHS1a; (**e**) 0.2 μg of cDNA corresponding to A_1R; or (**f**) 0.15 μg of cDNA corresponding to $A_{2A}R$. Cells were also transfected with 2 μg of cDNA corresponding to the α-subunit of G_i fused to Rluc and increasing amounts of cDNA corresponding to the α-subunit of G_s fused to YFP (a) or 0.3 μg of cDNA corresponding to the γ-subunit fused to Rluc and increasing amounts of cDNA corresponding to the γ-subunit fused to YFP (b–f). Maximum miliBRET unit (*mBU*) values are the mean ± standard error of the mean of four different experiments. A scheme showing the protein to which Rluc and YFP were fused is provided (*top*). ***$p < 0.001$ by one-way ANOVA with post - hoc Dunnett's test

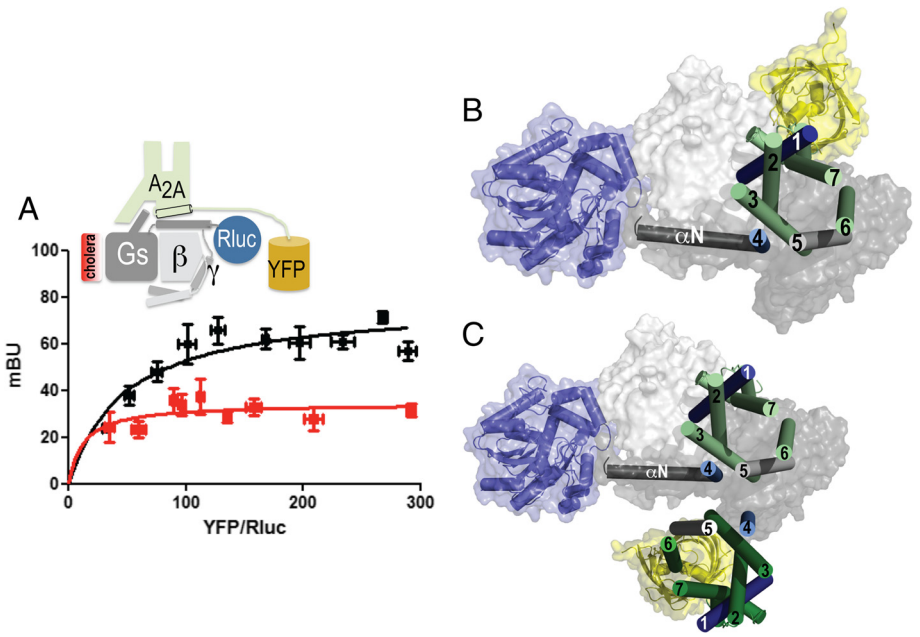

Fig. 4 Orientation of a G protein in a receptor homodimer. Bioluminescence resonance energy transfer (BRET) saturation experiments were performed in HEK-293T cells transfected with 2 μg of cDNA corresponding to the α-subunit of G_s fused to Rluc and increasing amounts of A_{2A}R-YFP (0.1–0.5 μg) cDNA. **a** BRET measurements in cells pretreated for 16 h with medium (*black line*) or with 100 ng/ml of cholera toxin (*red line*). Both fluorescence and luminescence of each sample were measured before every experiment to confirm similar donor expressions (approximately 50,000 bioluminescence units) while monitoring the increase in acceptor expression (1000–10,000 fluorescence units). miliBRET unit (*mBU*) values are the mean ± standard error of the mean of four to five different experiments grouped as a function of the amount of BRET acceptor. A scheme of the placement of donor and acceptor BRET moieties is provided (*top*). **b** Molecular model of the A_{2A}R-G_s complex. Rluc (*blue*) is attached to the N-terminal αN helix of G_s (*gray*), and YFP (*yellow*) is attached to the C-terminal domain of A_{2A}R (*light green*) (see Additional file 9: Figure S9 for details). **c** Arrangement of A_{2A}R homodimers modeled via the TM4/5 interface as observed in the oligomeric structure of β_1-AR [4]. The A_{2A}R protomer bound to α_s is shown in *light green*, whereas the second A_{2A}R-YFP protomer is shown in *dark green*. The molecular model in panel c (BRET between Rluc in G_s α subunit and YFP in a second A_{2A}R protomer; center-to-center distance between Rluc and YFP of 6.5 nm), in contrast to the model shown in panel B (BRET between Rluc in G_s α subunit and YFP in the G-protein bound A_{2A}R protomer; center-to-center distance between Rluc and YFP of 8.3 nm), would favor the observed high-energy transfer (see panel a) between α_s-Rluc and A_{2A}R-YFP

the N-terminal fragment of Rluc8 was fused to A_1R (A_1R-nRluc8) and its C-terminal domain to A_{2A}R (A_{2A}R-cRluc8), which only upon complementation can act as a BRET donor (Rluc8). The BRET acceptor protein was obtained upon complementation of the N-terminal fragment of YFP Venus protein fused to A_1R (A_1R-nVenus) and its C-terminal domain fused to A_{2A}R (A_{2A}R-cVenus). When all four receptor constructs were transfected, we obtained a positive and saturable BRET signal ($BRET_{max}$ of 35 ± 2 mBU and $BRET_{50}$ of 16 ± 3 mBU) that was not obtained for negative controls (Additional file 5: Figure S5). Figure 5a, b shows that the hemi-donor (A_1R-nRluc8 and A_{2A}R-cRluc8) and the hemi-acceptor (A_1R-nVenus and A_{2A}R-cVenus) moieties, placed at the C-terminus of the receptors, can only complement if A_1R-A_{2A}R heterodimerization occurs via the TM5/6 interface. The TM4/5 interface for homodimerization and the TM5/6 interface for heterodimerization give a rhombus-shaped tetramer organization (Fig. 5a). Remarkably, cell pre-incubation with either pertussis or cholera toxins decreased the $BRET_{max}$ by 35 % (Fig. 5c), further suggesting that both G_s and G_i proteins bind to the A_1R-A_{2A}R heterotetramer.

We next evaluated, using computational tools, whether the proposed A_1R-A_{2A}R heterotetramer could couple to both G_i and G_s proteins. Clearly, the external protomers of the proposed A_1R-A_{2A}R heterotetramer can bind to G_i and G_s proteins (Fig. 5d). This model positions the α-subunits of G_i and G_s in close contact, facing the interior of the tetrameric complex, while the N-terminal α-helices of α_i and α_s point outside the complex. The N-terminal α-helices of the γ-subunits are in close proximity, facing the inside (Additional file 6: Figure S6), which explains the significant energy transfer observed between γ-Rluc and γ-YFP (Fig. 3, bar b). The model provides experimental insights into the structural arrangement of heteromers consisting of two GPCRs and coupled to two G proteins, the possibility of which has recently been discussed [25]. We used MD simulations to study the stability of this complex. Additional file 7:

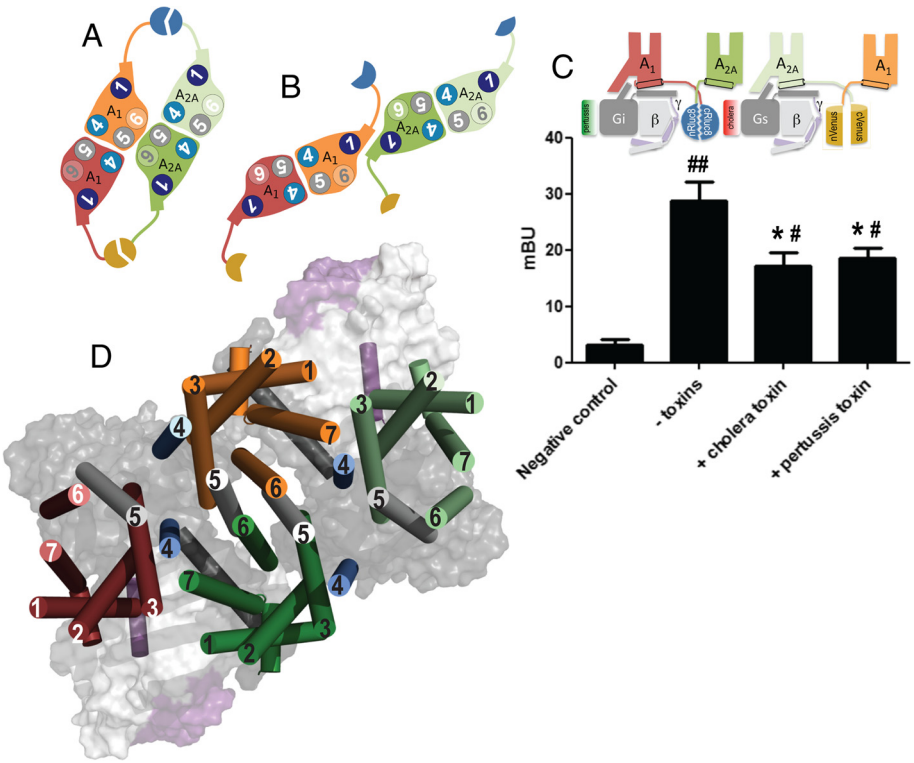

Fig. 5. Bioluminescence resonance energy transfer (BRET)-aided construction of a model consisting of G_i and G_s bound to an A_1R-$A_{2A}R$ heterotetramer. **a**, **b** A_1R-$A_{2A}R$ tetramer built using TM5/6 (a) or TM1 (b) inter-receptor interfaces modeled as in the structure of the μ opioid receptor [3]. TM helices 1, 4, and 5, involved in receptor dimerization, are highlighted in *dark blue*, *light blue*, and *gray*, respectively. nRluc8 and cRluc8 are shown in *blue* and nVenus and cVenus in *dark yellow*. **c** BRET and bimolecular fluorescence complementation experiments were performed in HEK-293T cells transfected with 1.5 μg of cDNA corresponding to A_1R-cRluc8 and $A_{2A}R$-nRluc8, and 1.5 μg of cDNA corresponding to A_1R-nVenus and $A_{2A}R$-cVenus. As the negative control, cells were transfected with 1 μg of cDNA corresponding to nRluc8 and 1.5 μg of cDNA corresponding to $A_{2A}R$-nRluc8, A_1R-nVenus, and $A_{2A}R$-cVenus. Cells were treated for 16 h with medium (– *toxins*), 10 ng/ml of pertussis toxin (+ *pertussis*), or 100 ng/ml of cholera toxin (+ *cholera*) prior to BRET determination. The relative amount of BRET is given as in Fig. 4 and values are the mean ± standard error of the mean of three different experiments. Student's t-test showed statistically significant differences with respect to the control ($^{\#}p < 0.05$, $^{\#\#}p < 0.01$) and a significant effect in the presence of either toxin over BRET in the absence of toxins ($^{*}p < 0.05$). A schematic representation at the *top* shows the protein to which the hemi luminescent or fluorescent proteins were fused. **d** Molecular model of the A_1R-$A_{2A}R$ tetramer in complex with G_i and G_s. A_1R bound to G_i is shown in *red*, G_i-unbound A_1R is shown in *orange*, $A_{2A}R$ bound to G_s is shown in *dark green*, G_s-unbound $A_{2A}R$ is shown in *light green*, and the α, β-, and γ-subunits of G_i and G_s are shown in *dark gray*, *light gray*, and *purple*, respectively. Transmembrane helices 4 and 5 are highlighted in *light blue* and *gray*, respectively

Figure S7 shows root-mean-square deviations (rmsd) on protein α-carbons throughout the MD simulation, as well as key intermolecular distances among protomers and G proteins. Clearly, both the A_1R protomer bound to G_i and the A_1R protomer that does not interact with it maintained a close structural similarity (rmsd ≈ 0.3 nm) relative to the initial structures. Similar results were obtained for the $A_{2A}R$ protomers (bound and unbound to G_s) (Additional file 7: Figure S7A). The fact that rmsd values of the whole system, formed by the A_1R-$A_{2A}R$ heterotetramer bound to G_i and G_s, are of the order of 0.6 nm indicates that the initial structural model is maintained during the MD simulation (Additional file 7: Figure S7A). As a consequence, selected intermolecular distances among protomers and G proteins remain constant during the MD simulation (Additional file 7: Figure S7B). A key aspect in the assembly of the heterotetramer is the TM interfaces for homodimerization (TM4/5) and heterodimerization (TM5/6). Additional file 8: Figure S8B shows rmsd values of the four-helix bundle forming the TM4/5 and TM5/6 interfaces, the initial and final snapshots of these bundles, and the evolution of the A_1R-$A_{2A}R$ heterotetramer during the MD simulation. Clearly, the rather small structural variations of these four-helix bundles, also reflected by rmsd <0.3 nm, suggest a stable complex. Notably, the TM5/6 four-helix bundle seems more stable than the TM4/5 bundles, as shown by its lower rmsd value. Additional file 8: Figure S8B, C depicts contact maps of the TM4/5 and TM5/6 interfaces, as well as the evolution of the network of hydrophobic interactions within these interfaces during the MD simulation.

Conclusions

For more than a decade, experimental evidence has supported the occurrence of homo-oligomers and hetero-oligomers of GPCRs [21]. However, our basic understanding of what makes heteromers different from homomers remains unknown. Our results, studying adenosine receptors as a model heteromer, point to three important new findings. First, the predominant stoichiometry in cells expressing A_1R-$A_{2A}R$ heteromers is 2:2; that is, a dimer of dimers (tetramer). Second, two different heterotrimeric G proteins can couple to heteromers, the overall complex constituting a functional unit. Third, the molecular orientation within the heteromer complex affords various qualitatively different interfaces; the two more relevant are the inter-protomer heteromeric interface and the inter-G-protein interface. Presumably, the two interfaces provide the key characteristic of heteromers: the ability of one protomer/G-protein complex to influence the signaling of the other. Surely, allosteric effects occurring between heteroreceptors and between G_s and G_i proteins are due to conformational changes transmitted along the intimately interacting molecules in the complex. In our controlled cell transfection system, which expressed a low density of receptors, minor species formed by monomers and trimers were found in addition to a predominance of tetramers in the plasma membrane, strongly supporting the occurrence of an in vivo dynamic distribution of receptors.

Adenosine was, from an evolutionary point of view, one of the first extracellular regulators given that it is involved in energy and nucleic acid metabolisms. Adenosine A_1 and A_{2A} receptors are expressed in almost every mammalian organ and tissue. In the heart, where adenosine plays a key role in both inotropic and chronotropic regulation, A_1R-mediated cardioprotection did not occur in $A_{2A}R$ knockout mice, suggesting an interaction between A_1 and A_{2A} receptors. In neurons, A_1 and A_{2A} receptors show co-localization, leading to inter-receptor interactions unveiled by pharmacological treatments. For instance, Okada et al. [27] showed that cAMP-dependent protein kinase A plays a role in the regulation of hippocampal serotonin release mediated by both A_1 and A_{2A} receptors. Similarly, the control of γ-amino butyric acid transport in astrocytes was attributed to the expression of A_1R-$A_{2A}R$ heteromers and to a specific mechanism by which the heteromer signals via G_i or G_s depending on the concentration of adenosine [28]. The structural basis of the differential signaling by the heteromer/G-protein macromolecular complex likely implies communication at the receptor-receptor level but also between G_s and G_i. Because the binding of two G proteins to a heterodimer is not feasible due to steric clashes [25], our finding that the A_1R-$A_{2A}R$ heterotetramer may bind to both G_s and G_i provides a structural framework to interpret experimental data.

Methods

Total internal reflection microscopy and single-particle data analysis

Single-particle imaging and tracking were performed on a Nikon Total Internal Reflection Fluorescence (TIRF) system, as detailed in Additional file 11: Supplementary Methods. Typically, 500 readouts of a 512 × 512-pixel region, the full array of the CCD chip, were acquired. For single-particle data analysis, parameters were calculated by applying the equations described in Additional file 11: Supplementary Methods.

Cell culture and transient transfection

HEK-293T cells were grow at 37 °C in Dulbecco's modified Eagle's medium (DMEM) (Gibco, Thermo Fischer Scientific, Madrid, Spain) supplemented with 2 mM L-glutamine, 100 U/ml penicillin/streptomycin, and 5 % (v/v) heat-inactivated fetal bovine serum (FBS) (all supplements were from Invitrogen, Paisley, UK). Cells were transiently transfected with cDNA corresponding to receptors, fusion proteins, $A_{2A}R$ mutants, or G-protein minigene vectors obtained as detailed in an expanded view by the polyethylenimine (PEI; SigmaAldrich, Cerdanyola del Vallès, Spain) method. Sample protein concentration was determined using a Bradford assay kit (Bio-Rad, Munich, Germany) using bovine serum albumin dilutions as standards. For single-particle imaging, cells were seeded into six-well plates containing glass coverslips (No. 1, round, 24 mm; Assistent, Sondheim, Germany) or into the Lab-Tek Chambered #1.0 Borosilicate Coverglass System (Nunc, Thermo Fisher Scientific, Schwerte, Germany). Cell transient transfections were performed with Lipofectamine™ 2000 (Invitrogen, Life Technologies, Darmstadt, Germany) or FuGENE 6 (Roche Applied Science, Indianapolis, IN, USA) and the application of 0.1–0.2 μg plasmid DNA per well. Before each experiment, cells were washed three times with 200 μL phenol red-free DMEM.

Plasmids

DNA sequences encoding amino acid residues 1–155 and 155–238 of YFP Venus protein, and amino acids residues 1–229 and 230–311 of RLuc8 protein were subcloned in the pcDNA3.1 vector to obtain the YFP Venus and RLuc8 hemi-truncated proteins. The human cDNAs for adenosine receptors, $A_{2A}R$ and A_1R, cloned into pcDNA3.1, were amplified without their stop codons using sense and antisense primers harboring unique EcoRI and BamHI sites to clone receptors into the pcDNA3.1RLuc vector (p*RLuc*-N1; PerkinElmer, Wellesley, MA, USA), and EcoRI and KpnI to clone $A_{2A}R$, A_1R, or GHS1a into the pEYFP-N1 vector (enhanced yellow variant of GFP; Clontech, Heidelberg, Germany). $G_{\alpha s}$ cloned into the *SFV1* vector, $G_{\alpha i}$ cloned into the pcDNA3.1 vector, or G_γ cloned into the *pEYFP-C1* vector were amplified

without their stop codons using sense and antisense primers harboring unique *Hind*III and *Bam*HI sites to clone them into the pcDNA3.1-Rluc vector, or EcoRI and KpnI to clone $G_{\alpha s}$ into the pEYFP-N1 vector. The amplified fragments were subcloned to be in-frame with restriction sites of the pcDNA3.1RLuc or pEYFP-N1 vectors to give plasmids that expressed proteins fused to RLuc or YFP on the N-terminal end ($G_{\alpha s}$-RLuc, $G_{\alpha i}$-RLuc, G_{γ}-RLuc, $G_{\alpha s}$-YFP, and G_{γ}-YFP) or the C-terminal end (A_1R-RLuc, $A_{2A}R$-RLuc, A_1R-YFP, $A_{2A}R$-YFP, and GHS1a-YFP). The human cDNAs for A_1R or GHS1a were subcloned into pcDNA3.1-nRLuc8 or pcDNA3.1-nVenus to give plasmids that expressed A_1R or GHS1a fused to either nRLuc8 or nYFP Venus on the C-terminal end of the receptor (A_1R-nRLuc8 and A_1R-nVenus or GHS1a-nRLuc8 and GHS1a-nVenus). The cDNAs for human A_{2A} or GHS1a receptors were subcloned into pcDNA3.1-cRLuc8 or pcDNA3.1-cVenus to give plasmids that expressed receptors fused to either cRLuc8 or cYFP Venus on the C-terminal end of the receptor ($A_{2A}R$-cRLuc8 and $A_{2A}R$-cVenus or GHS1a-cRLuc8 and GHS1a-cVenus). Expression of constructs was tested by confocal microscopy and the receptor-fusion protein functionality by measuring ERK1/2 phosphorylation and cAMP production, as described previously [13, 14, 17, 29].

"Minigene" plasmid vectors are constructs designed to express relatively short polypeptide sequences following their transfection into mammalian cells. Here, we used minigene constructs encoding the carboxyl-terminal 11-amino acid residues from G_{α} subunits of $G_{i1/2}$ (G_i minigene) or G_s (G_s minigene) G proteins; the resulting peptides inhibit G-protein coupling to the receptor and consequently inhibit the receptor-mediated cellular responses as previously described [24]. The cDNA encoding the last 11 amino acids of human G_{α} subunit corresponding to $G_{i1/2}$ (I K N N L K D C G L F) or G_s (Q R M H L R Q Y E L L), inserted in a pcDNA3.1 plasmid vector, were generously provided by Dr Heidi Hamm.

Energy transfer assays

For BRET and complementation BRET assays, HEK-293T cells were transiently cotransfected with a constant amount of cDNA encoding for proteins fused to RLuc, nRLuc8, or cRLuc8, and with increasing amounts of the cDNA corresponding to proteins fused to YFP, nYFP Venus, or cYFP Venus (see figure legends). To quantify protein-YFP expression or protein-reconstituted YFP Venus expression, cells (20 μg protein) were distributed in 96-well microplates (black plates with a transparent bottom) and fluorescence was read in a FLUOstar OPTIMA Fluorimeter (BMG Labtechnologies, Offenburg, Germany) equipped with a high-energy xenon flash lamp, using a 10 nm bandwidth excitation filter at 400 nm reading. Protein fluorescence expression was determined as the fluorescence of the sample minus the fluorescence of cells expressing the BRET donor alone. For BRET measurements, the equivalent of 20 μg of cell suspension were distributed in 96-well microplates (Corning 3600, white plates; Sigma) and 5 μM coelenterazine h (Molecular Probes, Eugene, OR, USA) was added. After 1 min for BRET or after 5 min for BRET with bimolecular fluorescence complementation, the readings were collected using a Mithras LB 940 that allows the integration of the signals detected in the short-wavelength filter at 485 nm (440–500 nm) and the long-wavelength filter at 530 nm (510–590 nm). To quantify protein-RLuc or protein-reconstituted RLuc8 expression, luminescence readings were also performed 10 min after adding 5 μM coelenterazine h. The net BRET was defined as [(long-wavelength emission)/(short-wavelength emission)] – Cf, where Cf corresponds to [(long-wavelength emission)/(short-wavelength emission)] for the donor construct expressed alone in the same experiment. BRET is expressed as miliBRET units (mBU; net BRET × 1000).

Computational model of the A_1R-$A_{2A}R$ tetramer in complex with G_i and G_s

The crystal structure of inactive $A_{2A}R$ [PDB:4EIY] [30] was used for the construction of human $A_{2A}R$ [UniProt:P29274] and A_1R [UniProt:P30542] homology models using Modeller 9.12 [31]. These receptors share 51 % of sequence identity and 62 % of sequence similarity, excluding the C-terminal after helix 8. Intracellular loop 3 (ICL3) of $A_{2A}R$ (Lys209–Gly218) and A_1R (Asn212–Ser219) were modeled using Modeller 9.12 [31] using ICL3 of squid rhodopsin [PDB:2Z73] as a template. The C-terminus tails of A_1R, containing 16 amino acids (Pro311–Asp326), and of $A_{2A}R$, containing 102 amino acids (Gln311–Ser412), were modeled as suggested for the oxoeicosanoid receptor (OXER) [32] (see Additional file 9: Figure S9 for details). The N-terminus of A_1R and $A_{2A}R$ were not included in the model. The "active" conformations of A_1R bound to G_i and $A_{2A}R$ bound to G_s were modeled using the crystal structure of β_2-AR in complex with G_s [PDB:3SN6] [33]. The globular α-helical domain of the α-subunit was modeled in the "closed" conformation [34], using the crystal structure of [AlF_4^-]-activated G_i [PDB:1AGR]. The location of YFP [PDB:2RH7] attached to the C-tail of $A_{2A}R$ was determined as suggested for the OXER [32] (see Additional file 9: Figure S9 for details). Rluc [PDB:2PSD] and YFP were fused to the to the N-terminus of the α-subunits and γ-subunits of G_i and G_s by a covalent bond. The structures of adenosine receptor oligomers were modeled via the TM4/5 interface for homodimerization, using the oligomeric structure of the β_1-AR [PDB:4GPO] [4], or via the TM5/6 interface for

heterodimerization, using the structure of the μ-OR [PDB:4DKL] [3]. The G_i-bound A_1R and G_s-bound $A_{2A}R$ protomers were rotated 10° to avoid the steric clash of the N-terminal helix of G_i and G_s with the C-terminal helix (Hx8) of G_s-unbound $A_{2A}R$ and G_i-unbound A_1R, respectively. This computational model, without Rluc and YFP, was placed in a rectangular box containing a lipid bilayer (814 molecules of 1-palmitoyl-2-oleoyl-sn-glycero-3-phosphocholine - POPC -) with explicit solvent (102,973 water molecules) and a 0.15 M concentration of Na^+ and Cl^- (1762 ions). This initial complex was energy-minimized and subsequently subjected to a 10 ns MD equilibration, with positional restraints on protein coordinates. These restraints were released and 500 ns of MD trajectory were produced at constant pressure and temperature (see Additional file 10: Movie M1). Computer simulations were performed with the GROMACS 4.6.3 simulation package [35], using the AMBER99SB force field as implemented in GROMACS and Berger parameters for POPC lipids. This procedure has been previously validated [36].

Availability of data and materials

The crystal structures 4EIY, 2Z73, 3SN6, 1AGR, 2RH7, 2PSD, 4GPO, and 4DKL are available from PDB (http://www.rcsb.org). All other relevant data are within the paper and its Additional files.

Additional files

Additional file 1: Figure S1. Examples of receptor trajectories in HEK-293T cells. Images of cells expressing A_1R-GFP (A) and of particular trajectories of A_1R-GFP-containing (B) or $A_{2A}R$-mCherry-containing (C) particles. (TIF 1164 kb)

Additional file 2: Figure S2. Graphical description of the stoichiometry of A_1R-GFP, $A_{2A}R$-mCherry or both A_1-GFP and A_{2A}-mCherry. The fluorescence intensity signal distribution (gray area) detected for more than 7000 independent observations is given for HEK-293T cells expressing A_1-GFP (A), A_{2A}-mCherry (D), or both A_1-GFP and A_{2A}-mCherry (B, E). The stoichiometry analysis was performed for A_1-GFP (A, B) and A_{2A}-mCherry (D, E). Curves approximately delineating the amount of monomers, dimers, trimers, and tetramers are displayed in green for A_1-GFP (A, B) and in red for A_{2A}-mCherry (D-E). The occurrence on the cell surface of monomers, dimers, trimers, and tetramers for A_1-GFP (C) expressed alone (black bars) or in the presence of A_{2A}-mCherry (blue bars) and for A_{2A}-mCherry (F) expressed alone (black bars) or in the presence of A_1-GFP (blue bars) was calculated by stoichiometry analysis from results shown in A, B, D, and E. (TIF 455 kb)

Additional file 3: Figure S3. Controls of cAMP production and BRET assays in cells expressing minigenes and in cells expressing the ghrelin GHS1a receptor instead of one of the adenosine receptors. (A,B) cAMP determination in HEK-293T cells transfected with (A) 0.3 μg of cDNA corresponding to A_1R or (B) with 0.2 μg of cDNA corresponding to $A_{2A}R$ with (control) or without 0.5 μg of cDNA corresponding to minigenes coding for peptides blocking either Gi or Gs binding. Cells were stimulated with the A_1R agonist N^6-Cyclopentyladenosine (CPA) (10 nM, red bars) in the presence of 0.5 μM forskolin (Fk) or with the $A_{2A}R$ agonist 4-[2-[[6-Amino-9-(N-ethyl-β-D-ribofuranuronamidosyl)-9H-purin-2-yl]amino]ethyl]benzenepropanoic acid hydrochloride (CGS-21680) (200 nM, blue bars). Values expressed as % of the forskolin-treated cells (CPA reduces forskolin-induced cAMP levels, red bars) or of the basal (CGS 21680 *per se* enhances cAMP levels, blue bars) are given as mean ± SD (n = 4–8). One-way ANOVA followed by a Bonferroni post - hoc test showed a significant effect of CPA when compared with that of forskolin (red bars, $^{***}p < 0.001$) or of CGS 21680 when compared to basal cAMP levels (blue bars, $^{\#\#}p < 0.01$, $^{\#\#\#}p < 0.001$). (C, D) BRET saturation curves were performed in HEK-293T cells transfected with (C) 0.3 μg cDNA coding for A_1R-Rluc, increasing amounts of cDNA coding for A_1R-YFP (0.1–1.5 μg cDNA), and 0.4 μg cDNA coding for GHS1a, or (D) with 0.2 μg of cDNA coding for $A_{2A}R$-Rluc, increasing amounts of cDNA coding for $A_{2A}R$-YFP (0.1–1.0 μg cDNA), and 0.5 μg cDNA coding for to GHS1a. Prior to BRET determination, cells were treated for 16 h with medium (black curves), with 10 ng/ml of pertussis toxin (green curves), or with 100 ng/ml of cholera toxin (red curves). mili BRET units (mBU) are given as the mean ± SD (n = 4–6 different experiments grouped as a function of the amount of BRET acceptor). (TIF 1418 kb)

Additional file 4: Figure S4. Possible interfaces in $A_{2A}R$ homodimers in complex with G_s. In A–E, the $A_{2A}R$ homodimer was modeled through TM4 using the H_1-receptor structure as template (A), through TM5 using the structure of squid rhodopsin (B), through TM4/5 using the β_1-receptor structure (C), and via TM5/6 (D) and TM1 (E) using the μ-OR structure. TM helices 1, 4, and 5 involved in receptor dimerization are highlighted in dark blue, light blue, and gray, respectively. $A_{2A}R$ protomers bound to G_s (in gray) are shown in light green, whereas G_s-unbound $A_{2A}R$ protomers are shown in dark green. Rluc (blue) is attached to the N-terminal αN helix of G_s, and YFP (yellow) is attached to the C-terminal domain of the G_s-unbound $A_{2A}R$ protomer (light green). It is important to note that the position of YFP is highly dependent on the orientation of the long and highly flexible C-tail of $A_{2A}R$ (102 amino acids, Gln311–Ser412), which was modeled as described for the OXER [32] (see Additional file 9: Figure S9 for details). Despite these limitations, we can crudely estimate the approximate distances between the center of mass of Rluc and YFP as 4.6, 10.1, 6.5, 11.6, and 8.3 nm for panels A–E, respectively. Thus, among all these possible dimeric interfaces, only the molecular models depicted in panels A (TM4 interface) and C (TM4/5 interface) would favor the observed high-energy transfer between G_s-Rluc and $A_{2A}R$-YFP (Fig. 4a in main paper). However, there is a steric clash between the N-terminal helix of Gs and the dark-green protomer in the TM4 interface. Accordingly, we have modeled $A_{2A}R$ homodimerization via the TM4/5 interface. Unfortunately, similar experiments with cells transfected with G_i-Rluc and A_1R-YFP could not be accomplished because of a lack of receptor expression (not shown); it is likely that the shorter C-tail of A_1R (16 amino acids, Pro311–Asp326) could not accommodate YFP in the presence of G_i in the right three-dimensional structure. The A_1R homodimer was built using the same TM4/5 interface as for $A_{2A}R$. (TIF 3135 kb)

Additional file 5: Figure S5. BRET assays in cells expressing fusion proteins containing hemi-Rluc8 and hemi-Venus moieties fused to adenosine receptors or containing the ghrelin GHS1a receptor instead of one of the adenosine receptors. (A) Saturation BRET curve in HEK-293T co-transfected with 1.5 μg of the two cDNAs corresponding to A_1R-cRLuc8 and $A_{2A}R$-nRLuc8 and with increasing amounts of cDNAs corresponding to A_1R-nVenus and $A_{2A}R$-cVenus (equal amounts of the two cDNAs). $BRET_{max}$ was 35 ± 2 mBU and $BRET_{50}$ was 16 ± 3 mBU. BRET in cells expressing cRluc8 instead of A_1R-cRluc8 gave a linear, non-saturable signal. (B) Comparison of BRET responses using complementary and non-complementary pairs, or replacing one adenosine receptor with the ghrelin GHS1a (gn) receptor. Data are mean ± SD of three different experiments grouped as a function of the amount of BRET acceptor. $^{***}p < 0.001$ with respect to BRET in cells expressing adenosine receptors and hemi-Rluc8 and hemi-Venus proteins. (TIF 398 kb)

Additional file 6: Figure S6. Details of the relative position of Rluc and YFP in a receptor heterotetramer interacting with two G proteins. Computational-based model of G_s and G_i bound to the adenosine A_1R-$A_{2A}R$ heterotetramer. Rluc and YFP fused to the N-terminal domain of the G_α-subunits point toward different positions in space (A), whereas Rluc and YFP fused to G_γ-subunits are close (B). The color code of the proteins is depicted in the adjacent schematic representations (TM4 and TM5 of GPCR protomers are in light blue and gray, respectively). (TIF 6445 kb)

Additional file 7: Figure S7. Molecular dynamics (MD) simulation of the adenosine A_1R-$A_{2A}R$ heterotetramer in complex with G_i and G_s. (A) Root-mean-square deviations (rmsd) on protein α-carbons of the whole system (black solid line), of the two A_1Rs (orange and red

solid lines), of the two A_{2A}Rs (light and dark green solid lines), of G_i (gray solid line), and of G_s (gray dotted line) throughout the MD simulation. This color scheme matches with the color of the different proteins depicted in the two adjacent schematic representations. (B) Intermolecular distances between the N-terminal helices of the γ-subunit of Gi and Gs (magenta line), the N-terminal helices of the α-subunit of G_i and G_s (gray line), the N-terminal helix of the α-subunit of G_i and the C-terminal helix (Hx8) of inactive A_1R (orange line), the N-terminal helix of the α-subunit of G_s and the C-terminal Hx8 of inactive A_{2A}R (green line), the C-terminal Hx8 of A_1R and A_{2A}R (blue lines). These computed intermolecular distances are depicted as double arrows in the two adjacent schematic representations. (TIF 6973 kb)

Additional file 8: Figure S8. Evolution of TM4/5 and TM5/6 interfaces as devised from MD simulations of the adenosine A_1R-A_{2A}R heterotetramer in complex with G_i and G_s. (A) Representative snapshots (20 structures collected every 25 ns) of the TM domains of A_1R bound to G_i (red), G_i-unbound A_1R (orange), A_{2A}R bound to G_s (dark green), and G_s-unbound A_{2A}R (light green). TM helices 4 and 5 are highlighted in light blue and gray, respectively. Initial (at 0 ns, transparent cylinders) and final (at 500 ns, solid cylinders) snapshots of TM interfaces are shown for homodimerization (TM4/5, within rectangles) and heterodimerization (TM5/6, within a circle) bundles. TM helices 4 (light blue), 5 (gray), and 6 (orange and green) are highlighted. (B) Root-mean-square deviations (rmsd) on protein α-carbons of the four-helix bundles forming the TM5/6 interface (orange solid line), TM4/5 interface of A_1R (blue dotted line), and TM4/5 interface of A_{2A}R (blue solid line) throughout the MD simulation. (C) Contact maps of the TM4/5 interface (rectangles in panel A) in the A_1R or A_{2A}R homodimer (left and right panels) and of the TM5/6 interface (circle in panel A) in the A_1R-A_{2A}R heterodimer (middle panel). Darker dots show more frequent contacts. (D) Detailed view of the extensive network of hydrophobic interactions (mainly of aromatic side chains) within the TM4/5 (left and right panels) and TM5/6 (middle panel) interfaces. The amino acids are numbered following the generalized numbering scheme of Ballesteros and Weinstein [37, 38]. This allows easy comparison among residues in the 7TM segments of different receptors. (TIF 4004 kb)

Additional file 9: Figure S9. Positioning YFP in the C-tail of A_{2A}R. The complex between the A_{2A}R protomer (in light green) and G_s (α-subunit in dark grey and yellow, β-subunit in light gray, and γ-subunit in purple) was constructed from the crystal structure of β_2 in complex with G_s [33]. Although the exact conformation of the A_{2A}R C-tail (102 amino acids, Gln311–Ser412) cannot unambiguously be determined, its orientation was modeled as in the C-tail of squid rhodopsin [39], which contains the conserved amphipathic helix 8 that runs parallel to the membrane and an additional cytoplasmic helix 9. Thus, the C-tail of A_{2A}R expands (see solid light green line) and points intracellularly toward the N-termini of the γ-subunit as suggested for OXER [32]. The laboratory of Kostenis has shown that the C-terminal of OXER, labeled with Rluc (OXER-Rluc), gets close to the N-terminal of the γ-subunit, labeled with GFP (γ-GFP) [32]. Analogously, we propose that YFP attached to the C-tail of A_{2A}R is positioned near the N-termini of the γ-subunit (in purple). (TIF 2395 kb)

Additional file 10: Movie M1. Assembly of adenosine A_1 and A_{2A} receptors in complex with two G proteins and MD simulation of the system. The assembly of G_s and G_i bound to the adenosine A_1R-A_{2A}R heterotetramer was subjected to 500 ns of MD simulation in a rectangular box containing the system, the lipid bilayer, explicit solvent, and ions. A_1R protomers are in orange and red, A_{2A}R protomers in light and dark green, G_α in white, G_β in gray, and G_γ in purple. For easier visualization of protomer-protomer interfaces, TMs 4 and 5 are highlighted in blue and white, respectively. (MPEG 87870 kb)

Additional file 11: Supplementary methods. (DOCX 72 kb)

Competing interests
The authors declare that they have no competing interests.

Authors' contributions
GN performed the molecular biology. GN, MB, EM, and DA perfomed BRET experiments. MZ-F performed single-particle tracking experiments. AC and LP-B performed molecular modeling studies. AC, VC, JM, and EIC analyzed the data. CL, LP, AJG-S, PJM, and RF designed the experiments, supervised the work in the respective laboratories and wrote the manuscript.. All authors read and approved the final manuscript.

Acknowledgments
We acknowledge the technical help provided by Jasmina Jiménez (CIBERNED, University of Barcelona). This study was supported by grants from the Spanish Ministerio de Ciencia y Tecnología (SAF2009-07276, SAF2010-18472, SAF2011-23813, SAF2013-48271-C2-2-R; those grants may include FEDER funds), the Max Planck Society, the German Cancer Research Center, and the German Ministry for Education and Research (BMBF). PJM and LP participate in the European COST Action CM1207 (GLISTEN). Authors gratefully acknowledge the computer resources provided by the Barcelona Supercomputing Center - Centro Nacional de Supercomputación.

Author details
[1]Centro de Investigación Biomédica en Red sobre Enfermedades Neurodegenerativas (CIBERNED), Madrid, Spain. [2]Institute of Biomedicine of the University of Barcelona (IBUB), Barcelona, Spain. [3]Department of Biochemistry and Molecular Biomedicine, Faculty of Biology, University of Barcelona, Barcelona 08028, Spain. [4]Laboratori de Medicina Computacional, Unitat de Bioestadística, Facultat de Medicina, Universitat Autònoma de Barcelona, 08193 Bellaterra, Spain. [5]Max Planck Institute for Intelligent Systems, Heisenbergstrasse 3, 70569 Stuttgart, Germany. [6]German Cancer Research Center, Bioquant, Im Neuenheimer Feld 267, 69120 Heidelberg, Germany. [7]Interfaculty Institute of Biochemistry, Hoppe-Seyler-Strasse 4, 72076 Tübingen, Germany. [8]School of Pharmacy, University of East Anglia, Norwich NR4 7TJ, UK.

Received: 26 September 2015 Accepted: 16 March 2016
Published online: 05 April 2016

References
1. Fung JJ, Deupi X, Pardo L, Yao XJ, Velez-Ruiz GA, Devree BT, et al. Ligand-regulated oligomerization of beta(2)-adrenoceptors in a model lipid bilayer. EMBO J. 2009;28:2384–92.
2. Albizu L, Cottet M, Kralikova M, Stoev S, Seyer R, Brabet I, et al. Time-resolved FRET between GPCR ligands reveals oligomers in native tissues. Nat Chem Biol. 2010;6:587–94.
3. Manglik A, Kruse AC, Kobilka TS, Thian FS, Mathiesen JM, Sunahara RK, et al. Crystal structure of the micro-opioid receptor bound to a morphinan antagonist. Nature. 2012;485:321–6.
4. Huang J, Chen S, Zhang JJ, Huang XY. Crystal structure of oligomeric β1-adrenergic G protein-coupled receptors in ligand-free basal state. Nat Struct Mol Biol. 2013;20:419–25.
5. Lane JR, Donthamsetti P, Shonberg J, Draper-Joyce CJ, Dentry S, Michino M, et al. A new mechanism of allostery in a G protein-coupled receptor dimer. Nat Chem Biol. 2014;10:745–52.
6. Vinals X, Moreno E, Lanfumey L, Cordomi A, Pastor A, de La Torre R, et al. Cognitive impairment induced by delta9-tetrahydrocannabinol occurs through heteromers between cannabinoid cb1 and serotonin 5-ht2a receptors. PLoS Biol. 2015;13:e1002194.
7. Kasai RS, Kusumi A. Single-molecule imaging revealed dynamic GPCR dimerization. Curr Opin Cell Biol. 2014;27:78–86.
8. Hern JA, Baig AH, Mashanov GI, Birdsall B, Corrie JE, Lazareno S, et al. Formation and dissociation of M1 muscarinic receptor dimers seen by total internal reflection fluorescence imaging of single molecules. Proc Natl Acad Sci U S A. 2010;107:2693–8.
9. Calebiro D, Rieken F, Wagner J, Sungkaworn T, Zabel U, Borzi A, et al. Single-molecule analysis of fluorescently labeled G-protein-coupled receptors reveals complexes with distinct dynamics and organization. Proc Natl Acad Sci U S A. 2013;110:743–8.
10. Kasai RS, Suzuki KG, Prossnitz ER, Koyama-Honda I, Nakada C, Fujiwara TK, et al. Full characterization of GPCR monomer-dimer dynamic equilibrium by single molecule imaging. J Cell Biol. 2011;192:463–80.
11. Vilardaga JP, Nikolaev VO, Lorenz K, Ferrandon S, Zhuang Z, Lohse MJ. Conformational cross-talk between alpha2A-adrenergic and mu-opioid receptors controls cell signaling. Nat Chem Biol. 2008;4:126–31.
12. Fribourg M, Moreno JL, Holloway T, Provasi D, Baki L, Mahajan R, et al. Decoding the signaling of a GPCR heteromeric complex reveals a unifying mechanism of action of antipsychotic drugs. Cell. 2011;147:1011–23.
13. Gonzalez S, Moreno-Delgado D, Moreno E, Perez-Capote K, Franco R, Mallol J, et al. Circadian-related heteromerization of adrenergic and dopamine D(4) receptors modulates melatonin synthesis and release in the pineal gland. PLoS Biol. 2012;10:e1001347.

14. Navarro G, Ferre S, Cordomi A, Moreno E, Mallol J, Casado V, et al. Interactions between intracellular domains as key determinants of the quaternary structure and function of receptor heteromers. J Biol Chem. 2010;285:27346–59.
15. Ferre S, Baler R, Bouvier M, Caron MG, Devi LA, Durroux T, et al. Building a new conceptual framework for receptor heteromers. Nat Chem Biol. 2009;5:131–4.
16. Venkatakrishnan AJ, Deupi X, Lebon G, Tate CG, Schertler GF, Babu MM. Molecular signatures of G-protein-coupled receptors. Nature. 2013;494:185–94.
17. Ciruela F, Casado V, Rodrigues RJ, Lujan R, Burgueno J, Canals M, et al. Presynaptic control of striatal glutamatergic neurotransmission by adenosine A1-A2A receptor heteromers. J Neurosci. 2006;26:2080–7.
18. Orru M, Bakesova J, Brugarolas M, Quiroz C, Beaumont V, Goldberg SR, et al. Striatal pre- and postsynaptic profile of adenosine A(2A) receptor antagonists. PLoS One. 2011;6:e16088.
19. Harms GS, Cognet L, Lommerse PH, Blab GA, Kahr H, Gamsjager R, et al. Single-molecule imaging of l-type Ca(2+) channels in live cells. Biophys J. 2001;81:2639–46.
20. Whorton MR, Bokoch MP, Rasmussen SG, Huang B, Zare RN, Kobilka B, et al. A monomeric G protein-coupled receptor isolated in a high-density lipoprotein particle efficiently activates its G protein. Proc Natl Acad Sci U S A. 2007;104:7682–7.
21. Ferre S, Casado V, Devi LA, Filizola M, Jockers R, Lohse MJ, et al. G protein-coupled receptor oligomerization revisited: functional and pharmacological perspectives. Pharmacol Rev. 2014;66:413–34.
22. Fredholm BB, IJzerman AP, Jacobson KA, Linden J, Muller CE. International Union of Basic and Clinical Pharmacology. LXXXI. Nomenclature and classification of adenosine receptors–an update. Pharmacol Rev. 2011;63:1–34.
23. Carriba P, Navarro G, Ciruela F, Ferre S, Casado V, Agnati L, et al. Detection of heteromerization of more than two proteins by sequential BRET-FRET. Nat Methods. 2008;5:727–33.
24. Gilchrist A, Li A, Hamm HE. G alpha COOH-terminal minigene vectors dissect heterotrimeric G protein signaling. Sci STKE. 2002;2002:pl1.
25. Cordomi A, Navarro G, Aymerich MS, Franco R. Structures for G-protein-coupled receptor tetramers in complex with G proteins. Trends Biochem Sci. 2015;40:548–51.
26. Mondal S, Johnston JM, Wang H, Khelashvili G, Filizola M, Weinstein H. Membrane driven spatial organization of GPCRs. Sci Rep. 2013;3:2909.
27. Okada M, Nutt DJ, Murakami T, Zhu G, Kamata A, Kawata Y, et al. Adenosine receptor subtypes modulate two major functional pathways for hippocampal serotonin release. J Neurosci. 2001;21:628–40.
28. Cristovao-Ferreira S, Navarro G, Brugarolas M, Perez-Capote K, Vaz SH, Fattorini G, et al. A1R-A2AR heteromers coupled to Gs and G i/0 proteins modulate GABA transport into astrocytes. Purinergic Signal. 2013;9:433–49.
29. Canals M, Marcellino D, Fanelli F, Ciruela F, de Benedetti P, Goldberg SR, et al. Adenosine A2A-dopamine D2 receptor-receptor heteromerization: qualitative and quantitative assessment by fluorescence and bioluminescence energy transfer. J Biol Chem. 2003;278:46741–9.
30. Liu W, Chun E, Thompson AA, Chubukov P, Xu F, Katritch V, et al. Structural basis for allosteric regulation of GPCRs by sodium ions. Science. 2012;337:232–6.
31. Marti-Renom MA, Stuart AC, Fiser A, Sanchez R, Melo F, Sali A. Comparative protein structure modeling of genes and genomes. Annu Rev Biophys Biomol Struct. 2000;29:291–325.
32. Blattermann S, Peters L, Ottersbach PA, Bock A, Konya V, Weaver CD, et al. A biased ligand for OXE-R uncouples Gα and Gβγ signaling within a heterotrimer. Nat Chem Biol. 2012;8:631–8. doi: 10.1038/nchembio.962. Epub 2012 May 27.
33. Rasmussen SG, DeVree BT, Zou Y, Kruse AC, Chung KY, Kobilka TS, et al. Crystal structure of the β2 adrenergic receptor-Gs protein complex. Nature. 2011;477:549–55.
34. Chung KY, Rasmussen SG, Liu T, Li S, DeVree BT, Chae PS, et al. Conformational changes in the G protein Gs induced by the β2 adrenergic receptor. Nature. 2011;477:611–5.
35. Pronk S, Pall S, Schulz R, Larsson P, Bjelkmar P, Apostolov R, et al. GROMACS 4.5: a high-throughput and highly parallel open source molecular simulation toolkit. Bioinformatics. 2013;29:845–54.
36. Cordomi A, Caltabiano G, Pardo L. Membrane protein simulations using AMBER force field and Berger lipid parameters. J Chem Theory Comput. 2012;8:948–58.
37. Ballesteros JA, Weinstein H. Integrated methods for the construction of three dimensional models and computational probing of structure-function relations in G-protein coupled receptors. Methods Neurosci. 1995;25:366–428.
38. Isberg V, de Graaf C, Bortolato A, Cherezov V, Katritch V, Marshall FH, et al. Generic GPCR residue numbers - aligning topology maps while minding the gaps. Trends Pharmacol Sci. 2015;36:22–31.
39. Murakami M, Kouyama T. Crystal structure of squid rhodopsin. Nature. 2008;453:363–7.